International Conference on Applied Energy 2020
Dec. 1 - Dec. 10, 2020, Bangkok / Virtual
Paper ID: 564

Characterization of Confined Water Evaporation in Porous Media

Yadong Zhang[1], Hongxia Li[1], Hongtao Zhang[1], Nahla Al Amoodi[2*], TieJun Zhang[1*]

1 Department of Mechanical Engineering, Khalifa University of Science and Technology, Abu Dhabi, UAE

2 Department of Chemical Engineering, Khalifa University of Science and Technology, Abu Dhabi, UAE

*Correspondence: nahla.alamoodi@ku.ac.ae, tiejun.zhang@ku.ac.ae

ABSTRACT

While phase change materials have been widely used for latent heat storage, water/ice is promising for cold energy storage due to its large latent heat. Characterizing phase change, either ice melting or water evaporation, within porous media is of great significance for efficient cold energy charging/discharging and enhanced energy storage, but it remains challenging because of the opaque nature of porous matrix. In this work, by combining the non-destructive NMR-MRI technology and pore-scale numerical simulation, we investigate the dynamics of water-vapor transition in porous medium with an average grain size of 150 μm. The transient water content and distribution are obtained from NMR transversal relaxation time T_2. The shifting of T_2 curve and MRI imaging results show uniform evaporation over the entire device, which implies cavitation-induced evaporation in homogenous porous medium. This is further elucidated from the COMSOL simulation, where we look into the water-vapor interface evolution during the evaporation process in a representative pore. Our insights on water phase change in porous media are also valuable to geothermal energy extraction.

Keywords: thermal energy storage, porous medium, evaporation, nuclear magnetic resonance (NMR).

NOMENCLATURE

Abbreviations	
PFM	Phase Field Model
PCMs	Phase change materials
CFD	Computational fluid dynamics
CPMG	Car-Purcell-Meiboom-Gill sequence
TE	Time interval between two successive samplings
NECH	The number of sampling in each detection
Symbols	
T_2	NMR transversal relaxation time of pore fluid
T_{2s}	NMR transversal relaxation time of fluid adhering on grain surface
$a.u.$	NMR signal amplitude
i	i^{th} sampling during one NMR detection
SR	Surface relaxivity of porous matrix
S/V	The ratio of fluid-grain surface contacting area to the volume of pore fluid
$\boldsymbol{u}$	Velocity of fluid
t	Time
ϕ	Phase field variable
ψ	Phase field help variable
γ	Fluid mobility, $\gamma = \chi\epsilon^2$
λ	Mixing energy density, $\lambda = 3\epsilon\sigma/\sqrt{8}$
σ	Water-vapor interfacial tension
ϵ	Parameter controlling the thickness of fluids interface
χ	Mobility tuning parameter
r	Curvature of fluids interface
$\Delta\rho$	Density difference of water and vapor, $\Delta\rho = \rho_{water} - \rho_{vapor}$
g	Gravitational acceleration
B_o	Bond number, $B_o = \Delta\rho g r^2/\sigma$.

Selection and peer-review under responsibility of the scientific committee of the 12th Int. Conf. on Applied Energy (ICAE2020).

1. INTRODUCTION

Energy storage plays a key role in adjusting the gap between energy supply and demand, and potentially promotes the development of renewable energy such as solar and wind power. Thermal energy storage has received increasing popularity in recent years owing to its potential in shifting energy demand [1,2], particularly for energy-intensive cooling applications [3-5]. One of the popular methods of storing cold energy is to use phase change materials (PCMs) in porous medium. PCMs are known for high-energy storage density and negligible temperature variation during phase change, while porous medium provides large heat-exchange surface area and good thermal conductivity. Phase change heat transfer of materials in porous media determines the latent heat storage performance, including charging/discharging speed and energy storage density.

One of the widely used PCMs for cold energy storage is water; water freezing into ice involves cold energy storage while ice melting and water evaporation are related to cold energy recovery. Upon the different applications, ice-water-vapor transition is indispensable in the extraction of geothermal energy resources stored in subsurface porous medium. Therefore, it is of great significance to elucidate this phase change behavior in porous medium. However, the opacity of porous medium, the complexity in 3D pore-throat network and the heterogeneity in surface wettability impose considerable difficulties.

Recent advances in low-field nuclear magnetic resonance (NMR) and magnetic resonance imaging (MRI) technology make it possible to probe physical insights without destroying the structure of opaque materials nor disturbing the actual phase change processes [6,7].

In this study, we apply NMR-MRI technology to characterize water-to-vapor phase change in homogeneous porous medium. Combining both experimental observation and numerical simulation, we investigate the dynamic behavior of the phase change process. In the experimental part, water-to-vapor transition is recorded by NMR transversal relaxation time T_2 and the transient water distribution in the entire porous medium is captured by MRI. Furthermore, for the evaporation in individual pore, we conduct two-phase flow simulation by using Phase Field Model (PFM) based on the robust finite element solver COMSOL Multiphysics. Our work provides insightful demonstration and deepens the understanding of water-to-vapor phase change in homogeneous porous medium.

2. METHODOLOGIES

2.1 NMR-MRI Technology

Nuclear magnetic resonance (NMR) refers to the response of atomic nucleus to external magnetic field. Due to its wide application in medical imaging, it is also known as magnetic resonance imaging (MRI). Since 1950s, NMR-MRI has been enormously applied in many areas [8-10]. In the field of porous medium, most attention goes to the NMR transversal relaxation time T_2 of pore fluid caused by the interaction of atomic nucleus with magnetic field. T_2 is commonly approximated as:

$$\frac{1}{T_2} \cong \frac{1}{T_{2s}} = SR\left(\frac{S}{V}\right) \quad (1)$$

The distribution of T_2 is related to pore characteristics such as pore size distribution and hence it is widely applied in various energy applications, including subsurface resource extraction.

In this work, a low-field nuclear magnetic resonance analyzer (NiuMag, MesoMR23-060H-I, permanent magnet: 0.5T, see Fig. 1a.) is used to characterize the phase change in porous media. This proton-based NMR analyzer accurately quantifies liquid water content and distribution along with MRI cross-section imaging.

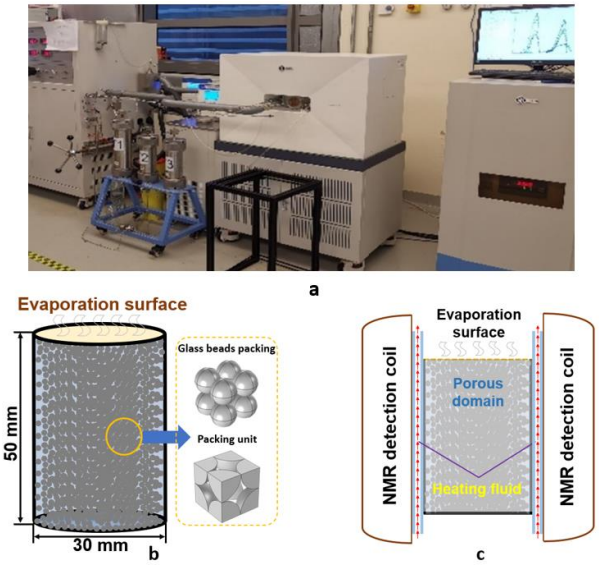

Fig 1 a. NMR-MRI analyzer; b. Sketch of porous medium; c. Cross-sectional depiction of in-situ experiment set-up.

2.2 Evaporation Experiments and Data Acquisition

The porous medium is made of glass beads with diameter of $100\sim200\ \mu m$ and surface contact angle ranging between and $15\sim25°$. A cylindrical container with $30\ mm$ in diameter and $50\ mm$ in length is filled with glass beads and then placed in a sonicator for two hours. The resulting tightly packed glass beads, as

depicted in Fig. 1b, is used as the homogeneous porous medium with well-controlled porosity, pore size and surface wettability. The porous medium is then evacuated for thirty minutes for air removal before being filled with distilled water. Thereafter, it is placed in the oven for preheating for two hours at $50\,°C$ with evaporation surface sealed. This is to make sure that there is no temperature variation during experiments. Finally, the porous medium is fixed into the NMR detection coil with heating fluid flowing through its lateral wall, see Fig. 1c.

During experiments, NMR data are collected by applying CPMG pulse sequence with echo time TE=$0.2\,ms$ and NECH=18000. In addition, MRI images are captured at four positions over the porous medium, as shown in Fig. 5a. Since NMR-MRI signal is only influenced by liquid water, the transient water content and distribution can be demonstrated by NMR T_2 relaxation and MRI images respectively.

NMR-MRI signal is recorded every 30 minutes with data collection time of approximately 5 minutes. The experiment lasts for 40 hours, a total of 65 groups of data are collected with water saturation ranging from 1.00 to 0.02.

2.3 Two-Phase Flow Simulation

Computational fluid dynamics simulation is performed with the finite element solver COMSOL Multiphysics. Considering the homogeneity of porous medium and the packing of glass beads, we assume that there is a repetitive minimum packing unit that can represent the porous medium in terms of phase distribution during the phase change process. For this purpose, we conduct simulations based on different packing units (here the cubic packing is presented, as shown in Fig. 1b, other forms of packing will be included in our future work). While the resulting demonstration is a rough approximation, it can provide insights on the dynamics of the phase change process. We will verify the viability of this approach in Part 3.

Since the process involves two phases, we apply PSM to show the transient phase distribution [11,12]. The motion of fluids is obtained by numerically solving continuity and Navier-Stokes equations. The relative importance of gravity and capillarity is also examined by evaluating the Bond number. The calculated Bond number is at the order of 10^{-5}, therefore, the gravity term is negligible compared with capillarity and thus it is dropped from the Navier-Stokes equation. The dynamic phase distribution is obtained by solving Cahn-Hilliard equation, which states:

$$\frac{\partial \phi}{\partial t} + \boldsymbol{u} \cdot \nabla \phi = \nabla \cdot \frac{\gamma \lambda}{\epsilon^2} \nabla \psi \tag{2}$$

$$\psi = -\nabla \cdot \epsilon^2 \nabla \phi + (\phi^2 - 1)\phi \tag{3}$$

Cohn-Hilliard equation tracks the diffusive interface that separates two immiscible fluids, while the diffusive interface is defined as the region where the dimensionless phase field variable ϕ jumps from -1 to 1. In this study, $\phi = -1$ and $\phi = 1$ denote vapor and water phase respectively.

3. RESULTS

3.1 Experimental Characterization based on NMR-MRI

The distribution of NMR transversal relaxation time T_2 and the corresponding signal amplitude during evaporation is shown in Fig. 2. The T_2 distribution reflects the water distribution while the NMR signal amplitude indicates transient water content through the calibrated correlation $y = 2871.7x$ with the value of R^2 at 0.9977. x and y denote water content and NMR signal amplitude respectively.

The blue curve of 100 % saturation shows the initial water content and distribution in the porous medium. One can see that there is a clear unimodal T_2 distribution, meaning the good homogeneity of the porous medium, as otherwise there would be at least two obvious modals. T_2 distribution under different water saturation is also plotted in Fig. 2. As expected, NMR signal amplitude is gradually decreasing along with evaporation. Fig. 3 shows the variation of mass of water and evaporation rate. It is found that the evaporation rate is retained at high level before 23 h after which it suddenly drops to a relatively low level. The mass of water declines sharply before 30 h where the slope begins to decrease.

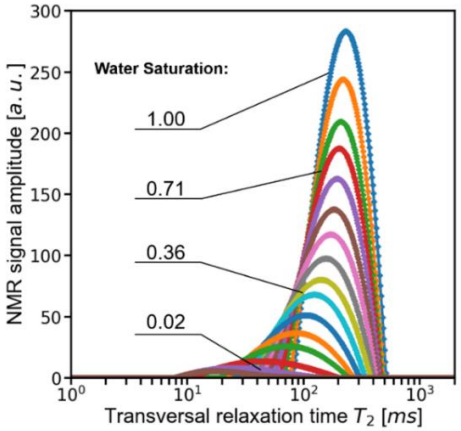

Fig 2 NMR signal amplitude and transversal relaxation distribution during water evaporation from porous medium.

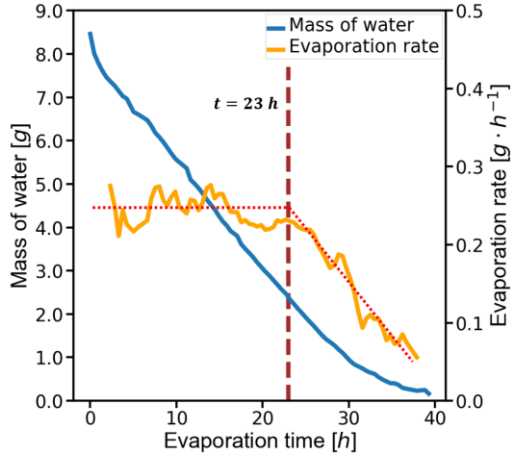

Fig 3 The variation of mass of water and evaporation rate along with evaporation. Red dashed lines represent the trend of evaporation rate.

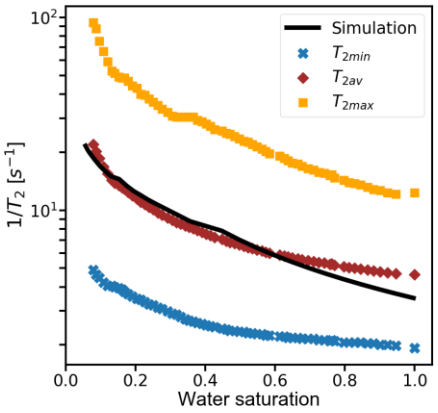

Fig 4 The variation of $1/T_2$ with water saturation. For the black curve, it is obtained by combining Eq. 1 and the value of S/V from simulation. The value of surface relaxivity is estimated at 80 $\mu m \cdot s^{-1}$.

Looking further into T_2 distribution, we notice that apart from the decline of NMR signal amplitude, the T_2 distribution gradually shifts towards lower T_2. Recalling Eq. 1, the shifting actually shows that the value of S/V is increasing, where a larger S/V value means less water remaining inside a pore. We also observe that T_{2min} and T_{2max}, the minimum and maximum T_2 value with non-zero NMR signal amplitude towards larger T_2, have similar shifting trend. For better demonstration, the variations of $1/T_{2\min}$ and $1/T_{2\max}$ with water saturation are plotted together as shown in Fig. 4. Since T_{2min} and T_{2max} are related to the minimum and maximum pore size, they should stand at fixed points if there is an evaporation front starting from the opening surface of porous medium and gradually receding into the inner area, which is widely claimed in previous studies [13,14]. Our observation, however, shows that there seems no obvious evaporation front at the device level, beyond which water is almost fully evaporated while the porous medium remains water saturated below that. Instead, it is more likely that evaporation happens uniformly over the entire porous medium.

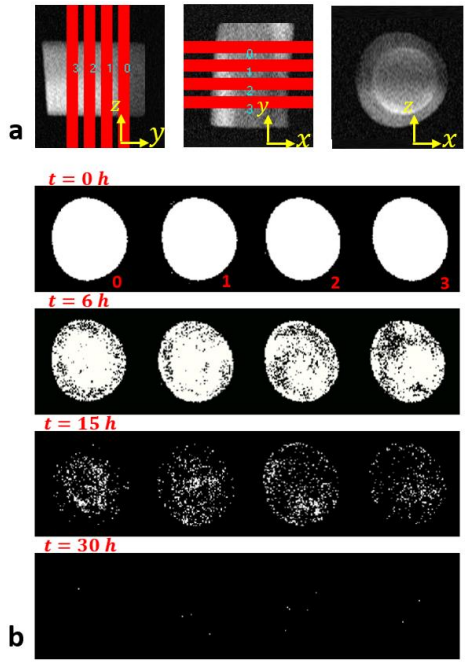

Fig 5 a. MRI imaging position. Slice 0 is the one closest to evaporation surface. b. MRI images of different slices during evaporation.

This finding is also supported by captured MRI images during the evaporation process, as shown in Fig. 5b. One can see that the brightness of all slices declines uniformly along with evaporation, even though they are at different depth of the porous medium. Since the brightness reflects water content and distribution, Fig. 5b is regarded as the direct evidence of uniform evaporation.

We assume that this phenomena is caused by cavitation in individual pores: During evaporation, vapor firstly generates from open surface which is directly connected to the ambient. Due to micro-sized pores and much smaller throats, the water-vapor meniscus generates a huge capillary pressure based on the Young-Laplace equation. Thus, water phase is under tension due to the negative pressure in the entire medium. Because the porous medium in our experiment is highly homogeneous, water cannot move to ease the tension, and hence cavitation slowly occurs. Furthermore, the uniform distribution of pore size leads to the uniform cavitation, which is then reflected as uniform evaporation in NMR data, as mentioned above. This cavitation-induced vaporization helps explain

experimental observation and it is supported by the simulation results as described in the following section.

3.2 CFD-based Numerical Simulation

We apply PSM simulating dynamic phase distribution within a cubic packing unit. For any given water saturation, we obtain the steady state phase distribution as well as the value of S/V. The phase distribution and fluid interface under different saturations are shown in Fig. 6. One can see that, as the evaporation proceeds, vapor bubble grows from the center of the unit pore and extends to throats gradually, which is well aligned with our analysis.

In addition, we observe two interesting phenomena. One is that, when evaporation reaches certain level, vapor in adjacent packing units connects together and thus water film is generated. To be specific, the packing unit is in fact hollow with water adhering on the grain surface. The other is, with continuous evaporation, water film begins to break and vapor gradually touches the grain surface. Finally, when the content of water is not enough to sustain film flow, vapor becomes fully connected while water is left only in corners. The above phenomena is related to the contact angle of grain surface. Specifically, the smaller the contact angle, the higher stability the water film. We will include more details in upcoming work.

We also conduct quantitative comparison between experimental and simulation results. On the one hand, we obtain the value of S/V from simulation and the equivalent $1/T_2$, which is specific to individual pore, by applying Eq. 1 (the value of surface relaxivity SR is estimated at $80\ \mu\text{m}\cdot\text{s}^{-1}$ while the exact value remains to be determined through experiment). Thereafter, we get the variation of the equivalent $1/T_2$ with water saturation. On the other hand, for the experimental data, we apply an average value, T_{2av}, to represent the overall T_2 distribution for any given water saturation. T_{2av} is obtained as:

$$lg\,T_{2av} = \frac{\Sigma_i (a.u.)_i \times lg\,T_{2i}}{\Sigma_i (a.u.)_i} \qquad (5)$$

Therefore, we have two groups of data showing the variation of $1/T_2$ with water saturation, one from simulation and the other from experiment. When compared with each other, see Fig. 4, one can see that there is acceptable consistency between experimental and simulation results, indicating the viability of the approach we apply in the process simulation.

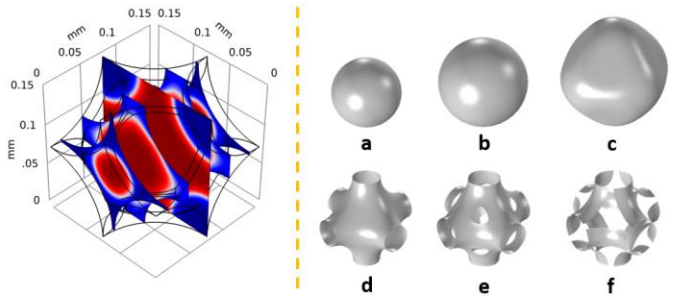

Fig 6 Simulation profile on the left is an example of phase distribution. Red and blue colored area represent vapor and water phase respectively. Figures on the right show phase interface during evaporation. a-c. vapor grows inside the pore; d. vapor bubble in adjacent units connects together and water film appears; e. vapor touches grain surface and water film begins to break; f. vapor is fully connected while liquid water is left in corners.

4. DISCUSSION

In this work, the cavitation-induced water vaporization along the entire porous medium is observed. However, it is rarely reported in previous studies, where an obvious evaporation front is claimed. One important reason for this discrepancy is the homogeneity of the porous medium. In our experiment, the porous medium is made of glass beads with similar diameter and hence it is of good homogeneity. After tight packing of the glass beads through the aforementioned method, the porous medium is able to have a narrow pore size distribution as demonstrated by the unimodal T_2 distribution. Further, the surface wettability of glass beads is well controlled and uniform over the porous medium, whereas in previous work, natural porous medium like soil or sand with impurities is directly used. As a result, neither of the above conditions is satisfied. The size of grain or glass beads ($150\ \mu\text{m}$ in average in diameter) also contributes to the discrepancy since it leads to much stronger capillarity than that reported in previous work, and the radial heating configuration over the entire device that we apply may strengthen the uniform cavitation too.

In terms of numerical simulation, we apply PSM to study phase change in a representative pore. We have studied the evolution of water-vapor interface and distribution and built up a link between pore-scale modeling and NMR T_2 measurements, but the precise value of surface relaxivity needs to be determined through experiment [15]. Currently, only the cubic packing is applied in simulation, other configurations of packing are studied in our ongoing work. Moreover, another important phase change behavior for cold

energy storage application, i.e., ice-water transition in porous medium, will also be investigated in our future research.

ACKNOWLEDGEMENT

This research is supported by the Khalifa University Competitive Internal Research Award (CIRA-2018-121) and Abu Dhabi Award for Research Excellence. The authors also appreciate great technical support from COMSOL Supporting Team.

REFERENCE

[1] Wu S, Yan T, Kuai Z, Pan W. Thermal conductivity enhancement on phase change materials for thermal energy storage: A review. Energy Storage Materials 2020;25:251-95.

[2] Stengler J, Linder M. Thermal energy storage combined with a temperature boost: An underestimated feature of thermochemical systems. Applied Energy 2020;262:114530.

[3] Li SF, Liu ZH, Wang XJ. A comprehensive review on positive cold energy storage technologies and applications in air conditioning with phase change materials. Applied Energy 2019;255:113667.

[4] Liu Z, Liu B, Guo J, Xin X, Yang X. Conventional and advanced exergy analysis of a novel transcritical compressed carbon dioxide energy storage system. Energy Conversion and Management 2019;198:111807.

[5] Mehari A, Xu ZY, Wang RZ. Thermal energy storage using absorption cycle and system: A comprehensive review. Energy Conversion and Management 2020;206:112482.

[6] Coates, GR, Xiao, L and Prammer, MG. NMR logging: principles and applications. Houston: Haliburton Energy Services; 1999.

[7] Song YQ, Venkataramanan L, Hürlimann MD, Flaum M, Frulla P, Straley C. T1–T2 correlation spectra obtained using a fast two-dimensional Laplace inversion. Journal of Magnetic Resonance 2002;154(2):261-8.

[8] Gore JC, Kang YS. Measurement of radiation dose distributions by nuclear magnetic resonance (NMR) imaging. Physics in Medicine & Biology 1984;29(10):1189.

[9] Pykett IL, Newhouse JH, Buonanno FS, Brady TJ, Goldman MR, Kistler JP, Pohost GM. Principles of nuclear magnetic resonance imaging. Radiology 1982;143(1):157-68.

[10] Rodriguez GG, Forte G, Anoardo E. Using Proton Nuclear Magnetic Resonance (NMR) as a calibrating reference for magnetic field measurement instruments: Sensitive volume and magnetic field homogeneity. Measurement 2020;151:107228.

[11] Steinbach I, Pezzolla F, Nestler B, Seeßelberg M, Prieler R, Schmitz GJ, Rezende JL. A phase field concept for multiphase systems. Physica D: Nonlinear Phenomena 1996;94(3):135-47.

[12] Singer-Loginova I, Singer HM. The phase field technique for modeling multiphase materials. Reports on progress in physics 2008;71(10):106501.

[13] Shokri N, Or D. What determines drying rates at the onset of diffusion controlled stage-2 evaporation from porous media? Water Resources Research 2011;47(9).

[14] Ben Neriah A, Assouline S, Shavit U, Weisbrod N. Impact of ambient conditions on evaporation from porous media. Water Resources Research 2014;50(8):6696-712.

[15] Slijkerman WF, Hofman JP. Determination of surface relaxivity from NMR diffusion measurements. Magnetic resonance imaging 1998;16(5-6):541-4.